



Trans. Nonferrous Met. Soc. China 33(2023) 3597-3611

Transactions of Nonferrous Metals Society of China

www.tnmsc.cn



## Correlation between grain structures and tensile properties of Al-Li alloys

Hao-ran LI<sup>1</sup>, Zhi-tao ZOU<sup>1</sup>, Jin-feng LI<sup>1,2</sup>, Guo-fu XU<sup>1,2</sup>, Zi-qiao ZHENG<sup>1</sup>

- 1. School of Materials Science and Engineering, Central South University, Changsha 410083, China;
- Key Laboratory of Nonferrous Metal Materials Science and Engineering, Ministry of Education, Central South University, Changsha 410083, China

Received 9 June 2022; accepted 7 September 2022

**Abstract:** The correlation of grain structures (texture and grain shape) of some Al–Li alloys to their yield strength (YS) and elongation was investigated from a new perspective. The investigated materials include 2195, 2A96, 2A55 and 2050 Al–Li alloy sheets with 2 mm in thickness and plates with 5 and 10 mm in thickness as well as different layers in 2297-T87 and 2050-T83 Al–Li alloy thick plates with 80–85 mm in thickness. Higher YS in general corresponds to higher average orientation factor  $M(\bar{M})$  values, but there still exist some exceptions. As yielding occurs during tensile deformation, some grains just rotate, slip systems are not activated in all grains and the activated slip system number in different grains is also different. The  $\bar{M}$  value calculation therefore should be corrected and normalized excluding the grains in which slip system is not activated and considering the easiest activated slip systems. Meanwhile, the grain shape also plays an important role in YS. Although almost full recrystallization occurs, the higher grain aspect ratio tends to enhance the YS because of less grain rotating and more activated slip systems. Furthermore, the total equivalent slip system number and grain shape affect the elongation in that higher total equivalent slip system number and lower grain aspect ratio correspond to larger elongation.

Key words: Al-Li alloy; yield strength; elongation; texture; grain shape; slip system

### 1 Introduction

Al-Li alloys possess better fatigue performance, higher specific stiffness and specific strength than traditional Al alloys [1]. These advantages have led to the 3rd generation Al-Li alloys being increasingly substituted for conventional 2××× and 7××× Al alloys in aerospace and spacecraft industries [1].

Al-Li alloys are strengthened by aging precipitates T1 (Al<sub>2</sub>CuLi),  $\delta'$  (Al<sub>3</sub>Li) and  $\theta'$  (Al<sub>2</sub>Cu), of which the precipitate types and strengthening effect are mainly dependent on Cu and Li concentrations [2,3]. In addition, micro-alloying elements also play an important role in controlling

the precipitate distribution. Since 1980s, through the adjustment of Cu and Li concentrations and the addition of micro-alloying elements Mg, Ag and Zn, a series of the 3rd generation Al–Li alloys were developed and applied [4–9]. The Al–Cu–Li alloys containing micro-alloying elements of Mg and Ag include 2195, 2050 and 2198 [5–7], and 2195 Al–Li alloy has been successfully applied in the external tank of space shuttles [10]. The Mg + Zn contained Al–Li alloy 2099 was invented and applied in airplane A380 [11,12]. The 4th generation super-high strength Al–Li alloys 2055 and 2A96 (or 2A55) containing Mg + Ag + Zn were invented in Alcoa and China in 2010s [13–15], which have great application potential in airplane structure.

It was also reported that there existed obvious

mechanical property discrepancy between Al-Li alloy sheets and plates with the same chemical composition but different thicknesses [16,17]. In addition, research indicated that Al-Li alloys possessed mechanical property anisotropy [18,19]. Meanwhile, inhomogeneous distribution in tensile properties through thickness was also found in many Al-Li alloy thick plates [20-22]. Our previous investigations showed that the strength of 2050 and 2297 Al-Li alloy thick plates along longitudinal direction at center layer (T/2 layer, T is the thickness) was higher than that at the surface layer or T/3-T/4 layer [23,24]. HAFLEY et al [25] also reported the similar strength distribution in 2050 Al-Li alloy thick plate. The above strength difference and anisotropy were usually attributed to the texture discrepancy between thin sheet and thick plate and among different layers in thick plate which caused different average Taylor factors or Schmid factors. It was usually considered that more deformation textures and larger Taylor factor or lower Schmid factor correspond to higher yield strength (YS) [16,24].

However, according to some references and our previous research [23–28], there also existed some inconsistencies. Some Al–Li alloys with higher Taylor factor possessed lower YS, but the corresponding explanation was not entirely convincing and some exceptions were directly ignored [23,24]. In addition, during the calculation of average Taylor factor, all texture components and the texture-free component were considered [23,24,26,29], and the YS difference was explained by the average Taylor factor. This is based on an assumption that five slip systems are activated in all grains under the macro-yielding stress, which may be inconsistent with the actual deformation. Furthermore, most research was concentrated on the

yield strength, but the elongation and ultimate tensile strength differences were not explained in detail.

For the above reasons, combined with our previous research results [16,17,23,24,28,30] and some new research results, the correlation between grain structures and tensile properties of some Al–Li alloys was comprehensively investigated from a new perspective.

# 2 Materials, experimental procedures and strength model

## 2.1 Materials and experimental procedures

The materials used in this work include 2195, 2A96, 2A55, 2297 and 2050 Al–Li alloys, and their the chemical compositions are shown in Table 1. The 2195 Al–Li alloys with two different compositions were fabricated in laboratory, and the other Al–Li alloys were provided by Southwest Aluminum (Group) Co., Ltd., China.

The alloy fabrication and final heat treatment processes are presented in Fig. 1. HR and CR refer to hot-rolling and cold-rolling, respectively. The aging parameters for some Al–Li alloy thin sheets with 2 mm in thickness and plates with 5 and 10 mm in thickness are shown in Table 2. For the 2050 Al–Li alloy sheet, the solutionized alloys with high heating rate and low heating rate are simplified as 2050-H and 2050-L, respectively. 2050-A alloy is referred to as the solutionized alloy following annealing at 400 °C for 2 h.

The as-received 2297 Al-Li alloy with 85 mm in thickness was in a T87 state. The 2050-T3 Al-Li alloy plate with 80 mm in thickness was provided by Southwest Aluminum (Group) Co., Ltd., China, and final T83 aging state was completed through artificial aging at 150 °C for 35 h in laboratory.

**Table 1** Chemical compositions of used Al–Li alloys (wt.%)

			, (					
Alloy	Cu	Li	Mg	Ag	Zn	Zr	Mn	Al
2195-1	4.11	0.88	0.4	0.4	0.1	0.12	-	Bal.
2195-2	4.11	1.03	0.4	0.4	0.1	0.12	_	Bal.
2A96	3.81	1.28	0.4	0.4	0.4	0.11	0.3	Bal.
2A55	3.76	1.28	0.4	0.41	0.43	0.11	0.31	Bal.
2050	3.2-3.9	0.7 - 1.3	0.2 - 0.6	0.2 - 0.7	_	0.06 - 0.14	0.2 - 0.5	Bal.
2297	2.5-3.1	1.1 - 1.7	_	_	_	0.08 - 0.15	0.1-0.5	Bal.

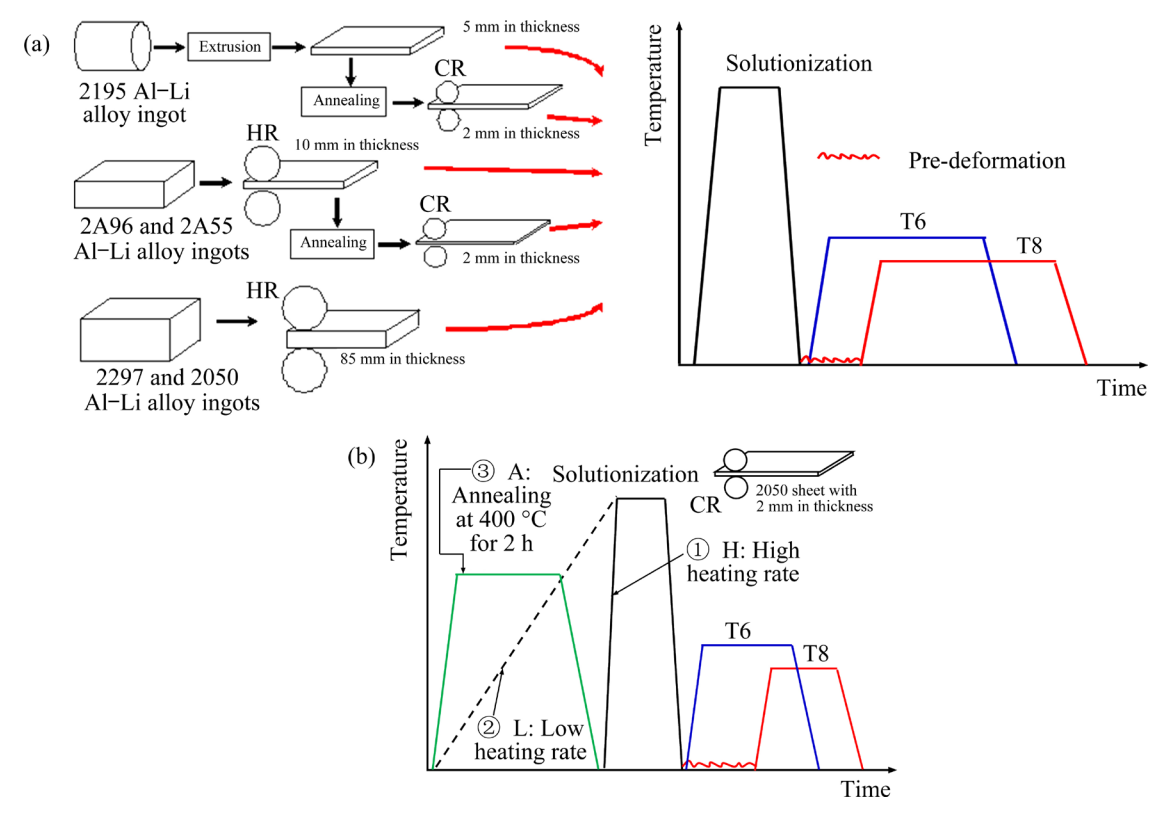


**Fig. 1** Alloy fabrication and final heat treatment processes for different Al–Li alloys: (a) 2195, 2A96 and 2A55 Al–Li alloy sheets with 2 mm in thickness and plates with 5 and 10 mm in thickness as well as 2297 and 2050 Al–Li alloy thick plates; (b) 2050 Al–Li alloy sheet with 2 mm in thickness

**Table 2** Aging parameters of some Al-Li alloy thin sheets with 2 mm in thickness and plates with 5 and 10 mm in thickness

Alloy	Aging type	Pre- deformation	Temperature/ °C	Time/
2195	T8	3.8%-stretch	148	45
2406	T6	0	175	24
2A96	T8	3.0%-stretch	150	30
2A55	T8	3.8%-stretch	148	35
2050	T6	0	175	26
2050	Т8	5.0%-cold rolling	155	32

Tensile properties of different Al–Li alloy sheets and plates and different layers in Al–Li alloy thick plate along the longitudinal direction were measured. The sampling positions for the 2297 and 2050 Al–Li alloy thick plates are shown in Fig. 2. Tensile sample appearance and dimensions for different alloys are shown in Table 3. Textures were measured through X-ray diffraction (XRD) and analyzed, detailed texture measurements can also be seen in Refs. [16,17,23,24,30]. In addition, the metallography was observed. The polished samples

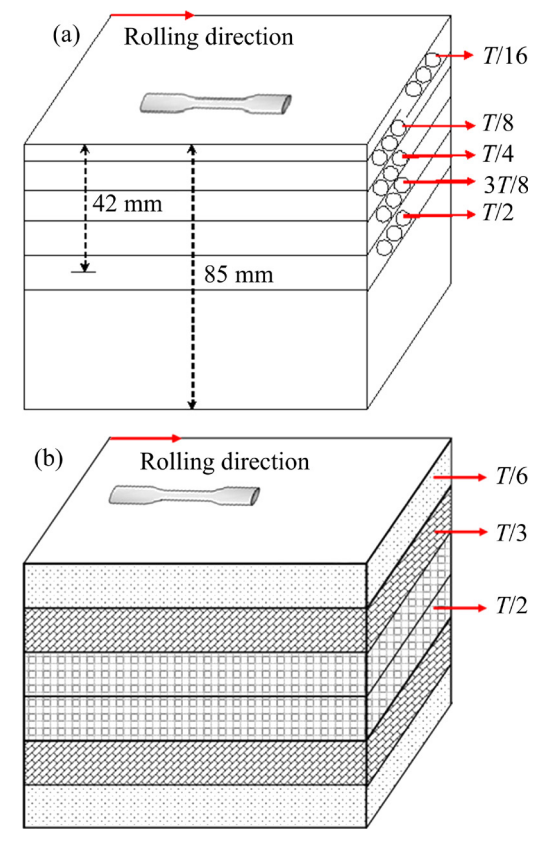


**Fig. 2** Sampling positions for Al–Li alloy thick plates: (a) 2297 Al–Li alloy; (b) 2050 Al–Li alloy [23]

**Table 3** Tensile appearance and dimensions for Al–Li allovs with different thicknesses

anoys with	different times	KIICBBCB		
Thickness/	Sample	Length/	Width/	Diameter/
mm	appearance	mm	mm	mm
2	Sheet	30	8	_
5	Plate	50	12.5	_
10	Rod	25	_	5
80, 85	Rod	25, 40	_	5, 8

for metallograhical observations were firstly anodically treated in a solution containing 1.1 g  $H_3BO_3$ ,  $95 \text{ mL } H_2O$  and 3 mL HF, and then the metallograhical observations were performed with an optical microscopy.

## 2.2 Yield strength model

The macroscopic YS ( $\sigma_y$ ) of polycrystalline metals can be related to the critical resolved shear stress (CRSS) of the crystals through Eqs. (1) and (2) [31–33]:

$$\sigma_{y} = \Delta \sigma_{gb} + M \tau_{tot}$$
 (1)

$$\tau_{\text{tot}} = \Delta \tau_0 + \Delta \tau_{\text{ss}} + \Delta \tau_{\text{d\&ppt}} \tag{2}$$

where  $\Delta \sigma_{\rm gb}$  is the strengthening effect due to the presence of (sub-)grain boundaries; M is the orientation factor (sometimes refers to the Taylor factor) that depends on texture and the orientation of the tensile axis relative to the main axis of the worked specimen;  $\tau_{tot}$  is the total of the CRSS of pure matrix metal and strengthening contribution from solute atoms, pre-deformation and precipitates;  $\Delta \tau_{\rm ss}$  is the solid solution strengthening effect and is a function of equilibrium solute concentration at the ageing temperature;  $\Delta \tau_0$  is the CRSS of pure Al;  $\Delta \tau_{\text{d&ppt}}$ , the largest contribution to the strength of Al-Cu-Li alloys, comes from dislocations within the grain  $(\Delta \tau_d)$  and precipitation strengthening  $(\Delta \tau_{ppt})$ . For a T8-aged Al–Li alloy,  $\Delta \tau_d$  is increased, while  $\Delta \tau_{\rm ppt}$  is decreased with increasing the pre-deformation. There were some reports that the  $\Delta \tau_d$  is higher than  $\Delta \tau_{\rm ppt}$  at a higher pre-deformation [34–36].

There are some different models to calculate the M values of specific textures, assuming that the

number of activated slip systems is different. Table 4 shows the M values of specific texture in FCC metals along longitudinal direction based on Sachs model (1 system activated), Hutchinson model (3.5 systems activated) and Taylor model (5 systems activated) [31–33].

## 3 Results

### 3.1 Tensile properties

3.1.1 Tensile properties of Al-Li alloy fabricated through different deformation processes and heat treatments

Figure 3 shows two representative tensile curves of 2195-2 Al–Li alloy fabricated through hot-extrusion (5 mm in thickness) and cold-rolling (2 mm in thickness) after the same T8 aging, which intuitively displays their different mechanical properties. The specific longitudinal YS, ultimate tensile strength (UTS) and elongation values of the two T8-aged 2195 Al–Li alloy plates with 5 mm in thickness and sheets with 2 mm in thickness are shown in Table 5 [17,30]. To compare the tensile properties, the strength and elongation difference ( $\Delta X$ ) between the alloy with different thicknesses are also presented.

Table 6 shows longitudinal tensile properties of the super-high strength 2A96 and 2A55 Al-Li alloy sheets with 2 mm in thickness and plates with 10 mm in thickness after the same T8 and T6 peak-aging. The strength and elongation differences are also presented.

According to Table 5 and Table 6, for the Al-Li alloy with the same chemical composition but different thicknesses, some conclusions are summarized as follows. After the same T6 or T8 near peak-aging, the YS of Al-Li alloy plate fabricated through hot deformation (hot-rolling and extrusion) is much higher than that of the Al-Li alloy sheet fabricated through cold-rolling. Due to different sample appearances and dimensions, the measured elongation data can not reflect the absolute plasticity difference. However, it can still

Table 4 M values of specific textures along longitudinal direction in FCC metal based on three different models [31–33]

Model	System activated	Brass	Cu	S	Goss	Cube	R-Cube	Texture-free
Sachs	1	2.44	3.04	2.5	2.45	2.45	2.45	2.24
Hutchinson	3.5	2.94	3.44	2.97	2.45	2.45	2.45	2.6
Taylor	5	3.17	3.7	3.33	2.45	2.45	2.45	3.07

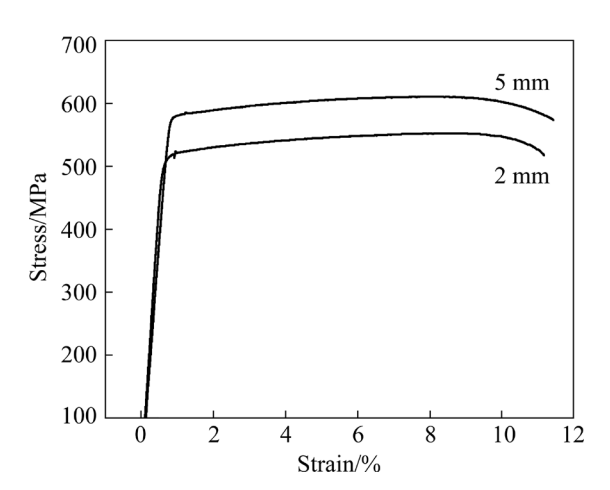


Fig. 3 Representative tensile curves of 2195-2 Al–Li alloy after same T8 aging

illustrate that the elongation of the plates with 5 and 10 mm in thickness is not larger, or even lower than that of the thin sheets with 2 mm in thickness after the same T6 and T8 peak aging.

Table 7 presents the longitudinal tensile properties of the T6- and T8-aged 2050 Al-Li alloy

thin sheet with different heat treatments prior to solutionization. The strength and elongation differences are also presented. It is special that in spite of the same solutionization holding stage and aging, different processes prior to solutionization cause great difference in the tensile properties of 2050 Al–Li alloy sheet. Annealing prior to solutionization (2050-A) and solutionization with low heating rate (2050-L) can greatly enhance the strength but lower the elongation of the T6- and T8-agaed 2050 Al–Li alloy sheet.

# 3.1.2 Tensile properties of Al-Li alloy thick plates at different locations through thickness

Table 8 and Table 9 show the longitudinal tensile properties of the 85 mm- and 80 mm-thick 2297-T87 and 2050-T83 Al-Li alloy plates at different 5 layers through thickness, respectively. It is obvious that the longitudinal strength at center layer is much higher than that at T/4-T/3 and T/16-T/6 layers, but the elongation is lowered. Considering the influence of hardenability (or lower cooling rate at the center during quenching), the

Table 5 Longitudinal tensile properties of two 2195 Al-Li alloys after same T8 aging

T :1		2195-1		2195-2				
Tensile property	2 mm	5 mm	$\Delta X_{(5 \text{ mm}-2 \text{ mm})}$	2 mm	5 mm	$\Delta X_{(5 \text{ mm}-2 \text{ mm})}$		
YS/MPa	529	577	48	532	586	54		
UTS/MPa	561	608	47	570	618	48		
Elongation/%	11.9	11.6	-0.3	12.1	10.6	-1.5		

**Table 6** Longitudinal tensile properties of super-high strength 2A96 and 2A55 Al-Li alloy plates with 2 and 10 mm in thickness after same T8 and T6 peak aging

		1 0	υ							
			2.	2A55						
Tensile property	2 mm		10	10 mm		$\Delta X_{(10 \text{ mm}-2 \text{ mm})}$		10 mm	$\Delta X_{(10 \text{ mm}-2 \text{ mm})}$	
	T6	Т8	Т6	Т8	Т6	Т8	Т8	Т8	Т8	
YS/MPa	559	563	591	641	32	78	561	600	39	
UTS/MPa	606	609	628	675	22	66	596	632	36	
Elongation/%	8.2	9	8.4	8.5	0.2	-0.5	10.9	9.5	-1.4	

**Table 7** Longitudinal tensile properties of T6- and T8-aged 2050 Al–Li alloy thin sheet with different heat treatments prior to solutionization

T1	2050-Н		2050-L	$\Delta X_{ m (L-H)}$	20:	50-A	$\Delta X_{ m (A-H)}$	
Tensile property	T6	T8 [28]	T8	T8	T6	T8 [28]	T6	Т8
YS/MPa	465	519	570	52	500	594	35	75
UTS/MPa	510	552	591	39	551	616	41	64
Elongation/%	9	8.3	6.2	-2.1	7.2	6.1	-1.8	-2.2

**Table 8** Longitudinal tensile properties of 85 mm-thick 2297-T87 Al–Li alloy plate at different layers through thickness [24]

Tensile	T/16	T/8	T/4	3 <i>T</i> /8	T/2	$\Delta X_{(T/2-T/8)}$
property						
YS/MPa	422	427	430	463	459	32
UTS/MPa	453	457	460	503	498	41
Elongation/%	12	15	11.5	9.5	9	-6

**Table 9** Longitudinal tensile properties of 80 mm-thick 2050-T83 Al–Li alloy plate at different layers through thickness [23]

Tensile property	<i>T</i> /6	<i>T</i> /3	<i>T</i> /2	$\Delta X_{(T/2-T/6)}$
YS/MPa	515	523	570	55
UTS/MPa	542	552	600	58
Elongation/%	13.5	11	9.6	-3.9

center layer should possess lower strength than the outside layers. However, the YS distribution is inconsistent with this consideration.

Because the tensile sample appearance and dimensions are the same, the elongation data therefore can reflect the absolute plasticity difference at different layers. It is found that the elongation at the center layer is much lower than that at the outer layers. For the 2297-T87 Al–Li alloy thick plate, the elongation at *T*/8 layer and *T*/2 layer is 15% and 9%, respectively. The elongation at *T*/6 layer and *T*/2 layer in the 2050-T83 Al–Li alloy thick plate is 13.5% and 9.6%, respectively.

## 3.2 Grain structures

Figure 4 presents three representative metallographic images on the longitudinal section of the Al-Li alloy sheets with 2 mm in thickness and plates with 5 and 10 mm in thickness. The first is featured by fine equi-axed grains (Fig. 4(a)), which appear in the 2050, 2A96 and 2A55 Al-Li alloy sheets with 2 mm in thickness after solutionization with high heating rate. The second is characterized with fiber-like un-recrystallized grains accompanied with a small number of fine equi-axed recrystallized grains (Fig. 4(b)), appearing in the hot rolled 2A96 and 2A55 Al-Li alloy plates with 10 mm in thickness and extruded 2195 Al-Li alloy plates with 5 mm in thickness after solutionization with high heating rate. The third is also featured by elongated grains (Fig. 4(c)), but the grain aspect on the longitudinal section is lower than that of the solutionized plates with 5 and 10 mm in thickness. This grain feature appears in the 2050-L and 2050-A samples.

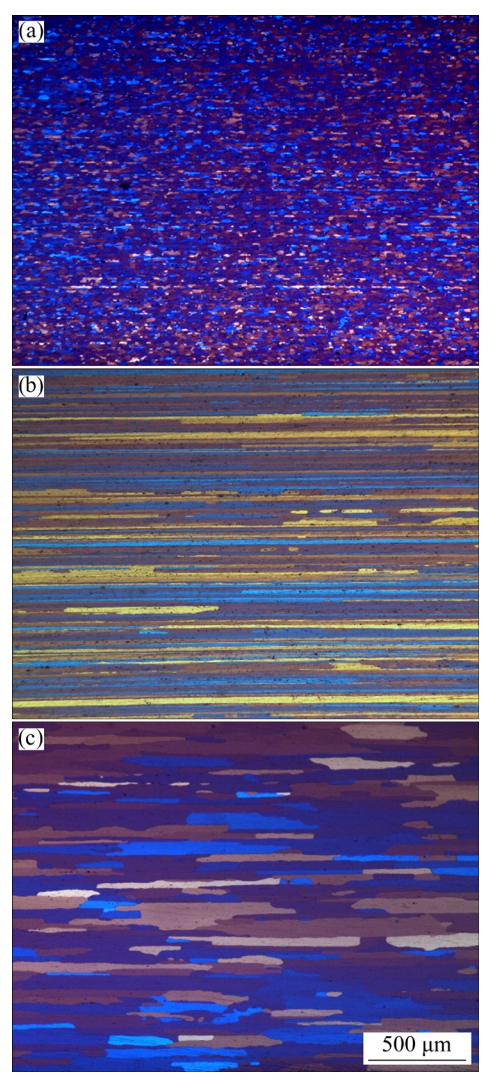
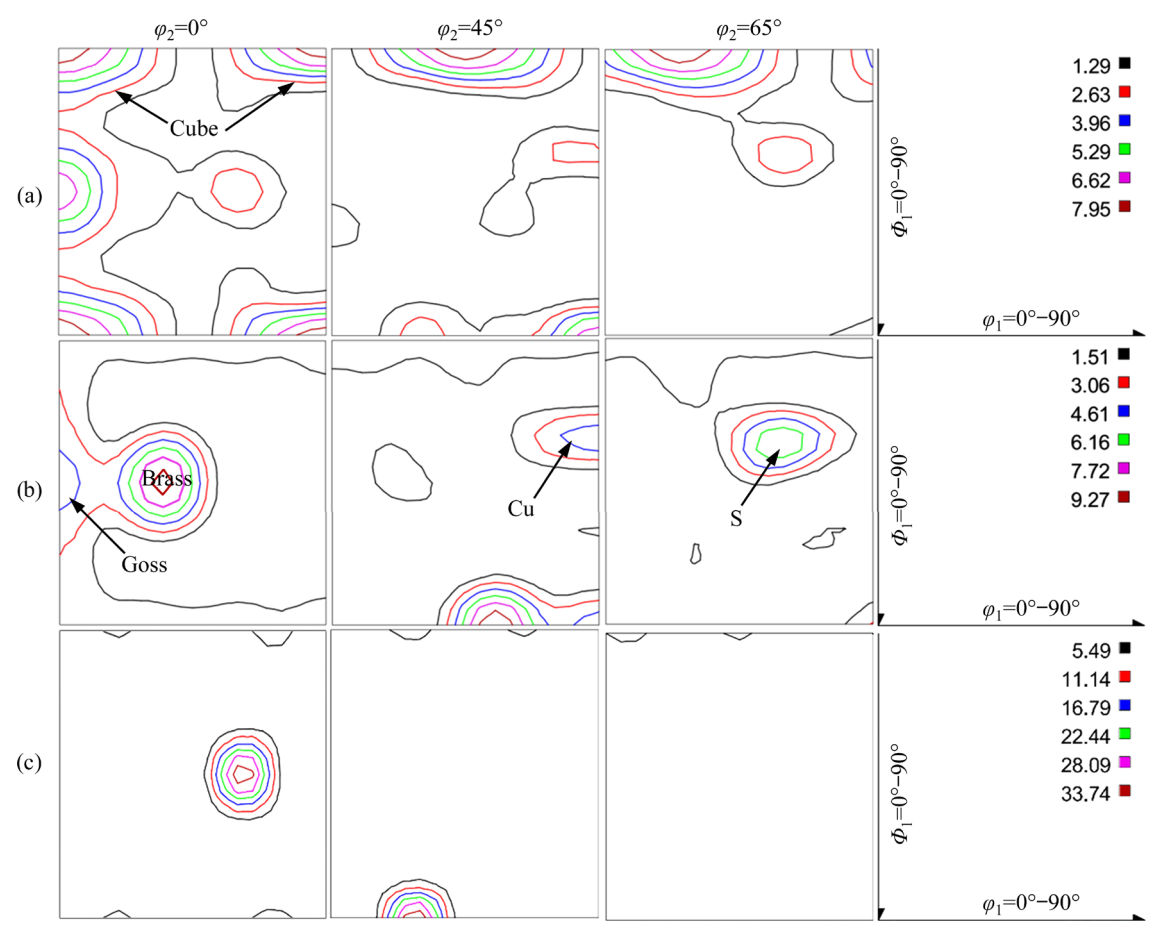


**Fig. 4** Representative metallographic images on longitudinal section: (a) Fine equi-axed recrystallized grains appearing in 2050, 2A96 and 2A55 Al–Li alloy sheets after solutionization with high heating rate; (b) Fiber-like un-recrystallized grains appearing in hot rolled 2A96 and 2A55 Al–Li alloy plates and extruded 2195 Al–Li alloy plate after solutionization; (c) Elongated but recrystallized grains in 2050-A and 2050-L samples

Different grain features are accompanied with different texture types and their specific volume fractions. Figure 5 shows three representative orientation distribution functions (ODFs) of the Al–Li alloy samples after solutionization or aging. The alloy consisting of fine equi-axed recrystallized

grains contains both deformation textures (Brass, S and Cu components) and recrystallization textures (Goss, Cube and R-Cube), and the alloy composed of fiber-like un-recrystallized grains includes obvious deformation textures, while there are no

obvious textures in the alloy comprised by elongated recrystallized grains. The analyzed volume fractions of various texture components and texture-free component in different Al–Li alloy sheets and plates after solutionization are shown in Table 10.



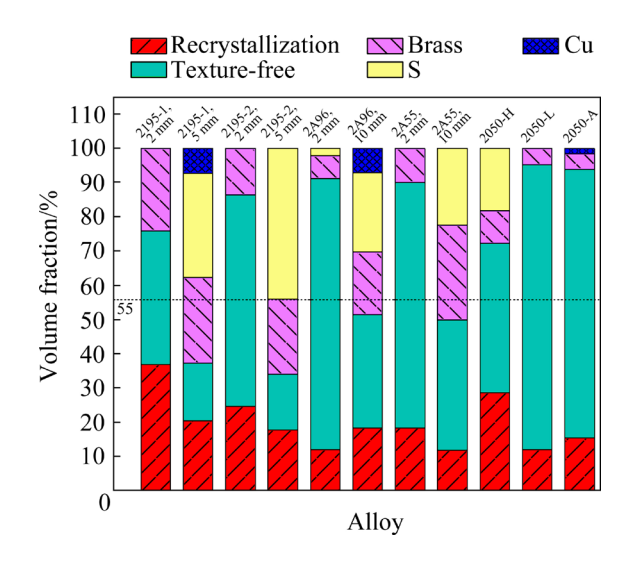
**Fig. 5** Representative ODFs of Al–Li alloy samples: (a) 2050 Al–Li alloy sheet after solutionization with high heating rate; (b) 2A96 Al–Li alloy plate after solutionization with high heating rate [16]; (c) 2050-A

Table 10 Volume fractions of various texture components in different Al-Li alloy sheets and plates after solutionization

A 11	Thickness/mm				V	olume f	raction/%		
Alloy 2195-1 [17] 2195-2 [30] 2A96 [16]	Tillexiless/IIIII	Brass	S	Cu	Goss	Cube	R-Cube	Recrystallization	Texture-free
2105 1 [17]	2	24.05	0	0	9.85	0	27.12	36.97	38.98
2193-1[1/]	5	25.02	30.26	7.39	0	16.26	4.16	20.42	16.91
2105 2 [20]	2	13.7	0	0	6.34	2.23	16.14	24.71	61.59
2193-2 [30]	5	21.98	44.04	0	0	17.78	0	17.78	16.2
2406 [16]	2	6.63	2.24	0	5.64	2.8	3.52	11.96	79.17
ZA90 [10]	10	18.42	23.1	7.07	10.53	6.03	1.67	18.23	33.18
2A55	2	10.06	0	0	3.04	9.89	5.35	18.28	71.66
2A33	10	27.73	22.43	0	4.42	7.36	0	11.78	38.06
2050-Н	2	9.65	18.19	0	13.56	11.11	3.96	28.63	43.53
2050-L	2	4.84	0	0	0	6.96	5.08	12.04	83.12
2050-A	2	4.7	0	1.53	7.89	3.3	4.34	15.53	78.24

In the order of recrystallization texture (Goss, Cube and R-Cube), texture-free component, Brass, S and Cu components according to the *M* values based on Hutchinson model and Taylor model, the stacked bar chart of volume fractions in different Al–Li alloy sheets and plates is then plotted, as shown in Fig. 6. It is clear that for the same Al–Li alloy, the total volume fraction of recrystallization textures and texture-free component is higher, or the total volume fraction of deformation texture is lower in the sheet than that in the plate, as indicated by 2195, 2A96 and 2A55 Al–Li alloys.

For the 2050 Al-Li ally sheet, different heat treatments prior to solutionization lead to grain feature variation. Solutionization with low heating



**Fig. 6** Stacked bar chart of volume fractions of various texture components in different Al–Li alloy sheets and plates after solutionization in order of recrystallization texture, texture-free component, Brass, S and Cu components

rate (2050-L) and solutionization following annealing at 400 °C for 2 h (2050-A) decrease the volume fraction of recrystallization and deformation textures, but greatly increase that of the texture-free component. As a result, the total volume fraction of recrystallization texture and texture-free component is greatly increased.

Table 11 shows the volume fractions of various textures and texture-free component at different layers in 2297-T87 and 2050-T83 Al–Li alloy thick plate through thickness. The corresponding stacked bar chart (Fig. 7) shows that the volume fraction of recrystallization texture from *T*/8 or *T*/6 layer to the center layer is decreased and that of deformation textures is increased. However, there seems no common law of total recrystallization texture and texture-free component for these two alloys.

#### 4 Discussion

## 4.1 Dependence of yield strength on texture

## 4.1.1 Difference between sheets and plates

Through comprehensively analyzing longitudinal tensile properties and components of the Al-Li alloy with the same compositions but different thicknesses (2, 5 and 10 mm), it is concluded that for the same T6 and T8 near peak aging, higher longitudinal corresponds to larger volume fraction deformation textures (Brass, S and Cu components) which to a large extent determines the average Mvalue of the corresponding alloy. A lot of research reports also attributed higher M value to higher YS [16-24]. Al-Li alloys in this paper are polycrystalline metals containing various textures

**Table 11** Volume fractions of various texture components at different layers in 2297-T87 [24] and 2050-T83 [23] Al–Li alloy thick plates through thickness (vol.%)

T			2050-T83					
Texture	T/16	T/8	T/4	3 <i>T</i> /8	T/2	T/6	T/3	T/2
Brass	21.78	13.96	18	26.51	24.16	12.78	6.21	9
S	7.02	0	11.67	35.56	19.58	12.88	3.21	21.43
Cu	13.05	0	4.98	0	9.9	20.27	1.58	13.27
Goss	9.59	2.77	8.34	9.47	10.38	17.03	3.09	8.48
Cube	6.17	27.96	14.1	5.87	2.66	22.32	12.93	9.03
R-Cube	3.63	14.23	0	0	3.28	0	5.38	0.99
Recrystallization	19.39	44.96	22.44	15.34	16.32	39.35	21.4	18.5
Texture-free	38.76	41.08	42.91	22.59	30.04	14.72	67.6	37.8

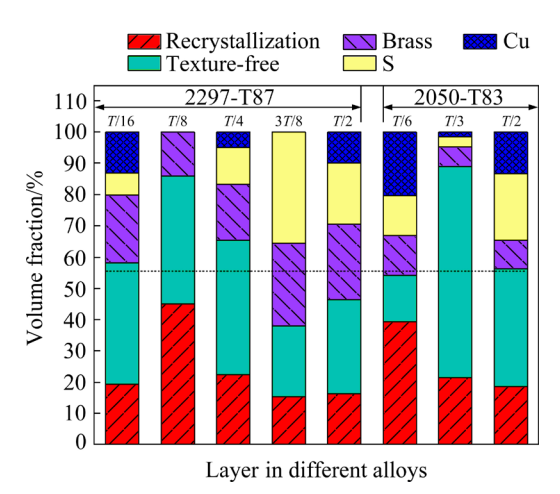


**Fig. 7** Stacked bar chart of volume fractions of various texture components at different layers in 2297-T87 and 2050-T83 Al–Li alloy thick plates through thickness after solutionization in order of recrystallization texture, texture-free, Brass, S and Cu components

and texture-free components, the average M value  $(\overline{M})$  can be calculated according to Eq. (3) [26].

$$\overline{M} = \sum_{i=1}^{n} (M_i F_i) + M_0 \cdot F_0$$
 (3)

where i describes the texture type and n refers to the number of textures in the sample,  $F_i$  is the volume fraction of a specific texture,  $M_0$  and  $F_0$  refer to the M value and volume fraction of texture-free component in the alloy sample, respectively. According to the M values of specific texture component based on Sachs model, Hutchinson model and Taylor model (Table 4), the  $\overline{M}$  values (simplified as  $\overline{M}_1$ ,  $\overline{M}_{3.5}$  and  $\overline{M}_5$ , respectively) for macroscopic loading along the longitudinal direction for the 2195, 2A96 and 2A55 Al–Li alloy sheets and plates are calculated, as shown in Table 12. It is clear that the plates with 5 and 10 mm in thickness possess higher  $\overline{M}_1$ ,  $\overline{M}_{3.5}$  and  $\overline{M}_5$  values than the sheets with 2 mm in thickness.

That is to say, the YS difference between the sheets and plates is consistent with the  $\overline{M}$  values for the 2195, 2A96 and 2A55 Al–Li alloys.

However, there exist some exceptions. The YS increments of T8-aged 2050-A and 2050-L are inconsistent with the calculated  $\overline{M}$  values. As shown in Table 13, the 2050-L and 2050-A sheets possess higher  $\overline{M}_5$  value but lower  $\overline{M}_1$  and  $\overline{M}_{3.5}$  values than the 2050-H sheet. Only  $\overline{M}_5$  values, but not  $\overline{M}_1$  and  $\overline{M}_{3.5}$  values can explain the YS difference.

All  $\overline{M}_1$ ,  $\overline{M}_{3.5}$  and  $\overline{M}_5$  values seem to be able to explain the YS difference from T/8 layer to T/2 layer in the 2297-T87 Al–Li alloy thick plate (Table 14). However, the YS at the surface layer (T/16 layer) is an exception, because of higher  $\overline{M}_1$ ,  $\overline{M}_{3.5}$  and  $\overline{M}_5$  values (Table 14) but lower YS at the T/16 layer than those at T/8 and T/4 layers (Table 8). In addition, the YS differences of the 2050-T83 Al–Li alloy thick plate are either unable to be explained by all the  $\overline{M}_1$ ,  $\overline{M}_{3.5}$  and  $\overline{M}_5$  values, because of higher  $\overline{M}_1$ ,  $\overline{M}_{3.5}$  and  $\overline{M}_5$  values (Table 15) but a little lower YS at the T/6 layer than those at T/3 layer (Table 9).

#### 4.1.2 *M* calculation correction

The above exceptions or contradictions indicate that some other factors are not taken into account. When the  $\overline{M}_1$ ,  $\overline{M}_{3.5}$  and  $\overline{M}_5$  values are calculated, it is assumed that dislocation slip is initiated in all grains with both textures and texture-free component, and the same number of slip systems are activated in all grains. In fact, not all grains are activated, and the activated slip system number in different grains is different as tensile yielding occurs, or even uniform plastic deformation is finished. It was reported that, only single and double sets of slip plane traces were clearly observed in a multicrystal Al–0.5%Mg alloy at 5%, 12% and 15% axial strain levels. This

**Table 12** Calculated  $\overline{M}$  values along longitudinal direction based on different models for 2195, 2A96 and 2A55 Al–Li alloy sheets and plates after solutionization

$ar{M}$	2195-1			2195-1			2A96			2A55		
				2 mm	5 mm	•	2 mm	10 mm	<b>*</b>	2 mm	10 mm	•
$\overline{M}_1$	2.37	2.47	Yes	2.32	2.44	Yes	2.28	2.43	Yes	2.30	2.38	Yes
$\overline{M}_{3.5}$	2.63	2.83	Yes	2.61	2.81	Yes	2.61	2.78	Yes	2.61	2.76	Yes
$\overline{M}_{5}$	2.86	3.09	Yes	2.93	3.10	Yes	3.01	3.08	Yes	2.97	3.08	Yes

 $\bar{M}_1$ ,  $\bar{M}_{3.5}$  and  $\bar{M}_5$  refer to  $\bar{M}$  values based Sachs model, Hutchinson model and Taylor model, respectively. Symbol  $\bullet$  refers to whether the calculated  $\bar{M}$  values are consistent with the YS difference

**Table 13** Calculated  $\overline{M}$  values for macroscopic loading along longitudinal direction based on different models for 2050 Al–Li alloy sheets with different solutionization processes

$\overline{M}$	2050-Н	2050-L	2050-A	•
${ar M}_1$	2.37	2.27	2.29	No
$ar{M}_{3.5}$	2.66	2.56	2.61	No
${ar M}_5$	2.95	3.00	2.99	Yes

**Table 14** Calculated  $\overline{M}$  values at different layers for macroscopic loading along longitudinal direction for 2297-T87 Al–Li alloy thick plate

$\overline{M}$	T/16	T/8	<i>T</i> /4	3 <i>T</i> /8	<i>T</i> /2	•
${ar M}_1$	2.45	2.36	2.39	2.42	2.45	No
$ar{M}_{3.5}$	2.78	2.58	2.71	2.80	2.81	No
$\overline{M}_{5}$	3.07	2.81	3.01	3.09	3.11	No

**Table 15** Calculated  $\overline{M}$  values at different layers for macroscopic loading along longitudinal direction for 2050-T83 Al–Li alloy thick plate

$\overline{M}$	T/6	T/3	T/2	<b>*</b>
$\overline{M}_1$	2.54	2.32	2.46	No
$\overline{M}_{3.5}$	2.80	2.61	2.79	No
${ar M}_{5}$	3.00	2.96	3.10	No

indicates that multicrystal Al obeys neither the Sachs nor the Taylor polycrystal deformation models, but deforms heterogeneously to favor easily slip transmission and accommodation among the grains [37]. It was also found that in Al-0.51Mg-0.76Si alloy sheet, plastic deformation within an individual grain was heterogeneous and slip systems activated in different grains were different [38]. In Ti<sub>6</sub>Al<sub>4</sub>V alloy with crystal structure different from that of Al alloy, it was observed that 55% slip systems were activated under macro-yielding stress [39]. To further verify the above assumption, the tensile samples of solutionized 2050-A and 2050-H were polished and subjected to a whole tensile process, then the polished surface with uniform macro-plastic deformation after fracture was observed by SEM, as shown in Fig. 8. Dislocation multislip traces were found in some grains in 2050-A (Figs. 8(a, b)), single slip rather than multislip was easily observed in 2050-H (Fig. 8(c)). In addition, the slip traces were not observed in some other grains of both 2050-A and 2050-H, even after a large plastic deformation, as indicated by the area surrounded by white dashed lines in Figs. 8(b) and (c). It can be concluded from Fig. 8 that the activated grains after a whole tensile process are lower than 90 vol.%. These observations further certify that not all grains are activated for dislocation slip at the time of macro-yielding and the activated slip system number in different grains is different.

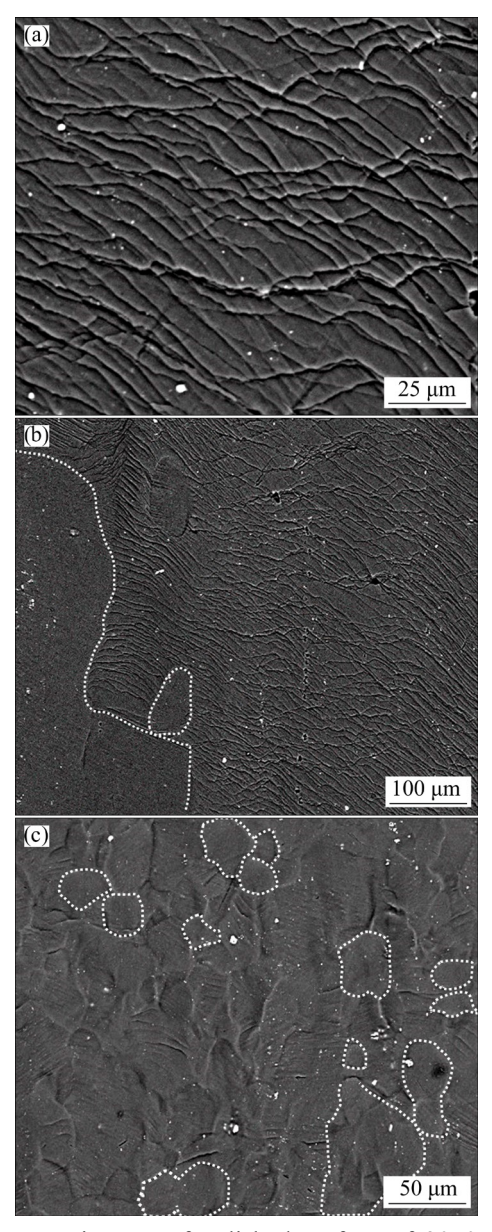


**Fig. 8** SEM images of polished surface of 2050 Al–Li alloy sheet after whole tensile process: (a, b) 2050-A; (c) 2050-H

During tensile deformation, dislocation slip in some grains is accompanied with grain rotation of the other grains without dislocation slip inside. It was pointed out that stress concentration led to grain rotation during deformation in Al-Mg-Zr alloy and the rotation degree increased with decreasing distance to the stress concentration location [40]. Because the grain boundary is the stress concentration location, the smaller grain size therefore means easier grain rotation during the tensile deformation.

Our observations (Fig. 8) and the previous research reports [37–40] indicate that the assumption of the same number of slip systems activated in all grains during deformation is incorrect. Therefore, no matter whether the calculated  $\overline{M}$  values in Tables 12–15 are consistent with the tensile property variation in Tables 5–9, the  $\overline{M}$  calculation should be corrected.

It is unable to exactly know how many grains and slip systems are activated under macro-yielding stress. However, according to the SEM observations in Fig. 8, the volume fraction of the activated grains should be much lower than 90 vol.% in the Al-Li alloy under macro-yielding stress. Here, it is assumed that dislocation slip is activated in grains with more than one half volume fraction but much lower than 90 vol.%, such as 55 vol.%. Meanwhile, according to Ref. [37], the Hutchinson model is used in the following re-calculation. In addition, the texture components are counted in the order of recrystallization texture, texture-free component, and Brass texture according to their specific M value order. If the total volume fraction of two components with lower specific M values is higher than 55 vol.%, other grains with higher specific M values are not counted. After normalization, the  $\overline{M}_{3.5}$  values for 2195, 2A96, 2A55 and 2050 Al-Li alloys thin sheet and plates with 5 and 10 mm in thickness are re-calculated, as shown in Table 16. Taking into account of fine equi-axed recrystallized grains in the aged 2195, 2A96, 2A55 and 2050-H sheets, the grains can rotate and the activated slip system number can be decreased, the  $\overline{M}_{3.5}$  values can be further lowered. It is illustrated that those corrected  $\overline{M}_{3.5}$  values are consistent with the YS variation in Tables 5–7.

However, the re-calculated  $\overline{M}_{3.5}$  values at different layers of the 2297-T87 and 2050-T83 Al-Li alloy thick plates after normalization by 55 vol.% (Table 17) are still a little inconsistent with the YS order. This inconsistency is characterized by  $\overline{M}_{3.5}$  values at T/16 layer in the 2297-T87 Al-Li alloy and at T/3 layer in the 2050-T83 Al-Li alloy. Considering the high total volume fraction of recrystallization texture and texture-free component with high ratio of texture-free component fraction to recrystallization texture fraction at T/16-T/4 layer in 2297-T87 plate and T/3 layer in 2050-T83 plate, and combined with the report that single and double sets of slip systems were activated in Al alloys during strain [37], the minimum  $\overline{M}_{3,5}$  value calculation can be further corrected according to the assumption that the Sachs model is applicable for the texture-free component. The corrected minimum  $\overline{M}_{3.5}$  values are indicated with the asterisk in Table 17.

#### 4.2 Effect of texture on elongation

A lot of research reports were concentrated on the correlation between YS and texture, but the tensile behavior and elongation should not be neglected. After the same aging, the elongation of the Al–Li alloy sheets is not lower, or even a little

**Table 16** Re-calculated  $\overline{M}_{3.5}$  values of 2195, 2A96, 2A55 and 2050 Al–Li alloy sheets and plates along longitudinal direction based on Hutchinson model after normalization by 55 vol.%

219	5-1	-1 2195-2		2A96		2A55		2050 sheet		
2 mm	5 mm	2 mm	5 mm	2 mm	10 mm	2 mm	10 mm	Н	L	A
2.53	2.69	2.56	2.69	2.58	2.65	2.60	2.70	2.54	2.58	2.58

**Table 17** Re-calculated  $\overline{M}_{3.5}$  values of 2297-T87 and 2050-T83 Al–Li alloy thick plates at different layers along longitudinal direction based on Hutchinson model after normalization by 55 vol.%

2297-T87						2050-T83	
T/16	T/8	<i>T</i> /4	3 <i>T</i> /8	T/2	T/6	<i>T</i> /3	T/2
2.55-2.31*	2.52-2.35*	2.55-2.31*	2.70	2.68	2.49	2.56-2.29*	2.55

<sup>\*</sup> For the texture-free component, the specific M values are based on Sachs model and Hutchinson model, due to its much higher fraction

higher than that of the Al–Li alloy plates with 5 and 10 mm in thickness, as shown in Tables 5–7. Actually, the solutionized sheets also possess higher elongation than the solutionized plate, as indicated in Fig. 9. In addition, the elongation at different layers in Al–Li alloy thick plate is different, which is characterized with lower elongation at center layer (Tables 8 and 9).

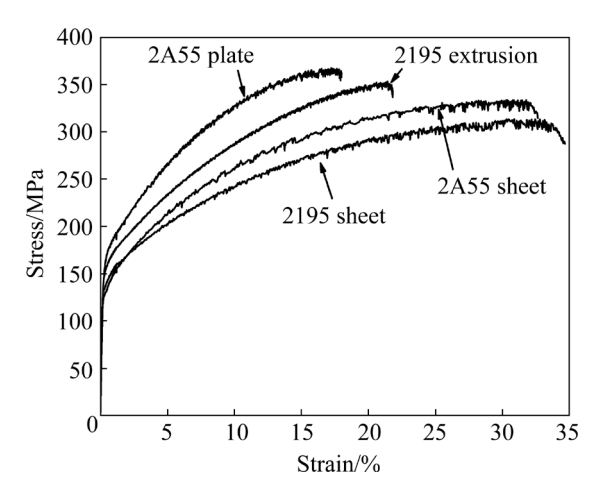


Fig. 9 Tensile curves of Al-Li alloy sheets and plates after solutionization

The elongation is mainly determined by the uniform plastic deformation, which is related to the dislocation slip. The activation of slip systems is dependent on the Schmid factor (SF). The slip system with the maximum SF (SF $_{max}$ ) is the easiest to be activated. For a specific texture, the SF $_{max}$  and its corresponding equivalent slip system number (ESSN) are shown in Table 18. Owing to the

requirements of deformation accommodation, the ESSN of polycrystalline alloy should be higher than 5, and the ESSN of the texture-free component is therefore assumed to be 5. The total ESSN (ESSN) of polycrystalline Al–Li alloy can be calculated according to Eq. (4) [41,42]:

$$\overline{\text{ESSN}} = \sum_{i=1}^{n} (\text{ESSN}_{i} \cdot F_{i}) + \text{ESSN}_{0} \cdot F_{0}$$
 (4)

where  $ESSN_0$  (=5) represents the ESSN of the texture-free component.

The calculated ESSN values of different Al–Li alloy sheets and plates and different layers in 2297-T87 and 2050-T83 Al–Li alloy thick plates are shown in Table 19 and Table 20, respectively. By comparing the elongation and ESSN of the same alloy with different thicknesses or at different layers in a thick plate, it is concluded that higher ESSN in general corresponds to lower volume fraction of deformation textures and larger elongation, because the deformation textures possess lower specific ESSN (Table 18). This regular pattern is applicable for the 2195, 2A96 and 2A55 Al–Li alloy sheets and plates as well as for different layers in the 2297 and 2050 Al–Li alloy thick plates.

However, there is also an exception for the 2050 Al–Li alloy sheet subjected to different solutionization treatments. After the same aging, the elongations of both 2050-L and 2050-A are lower, but their  $\overline{\text{ESSN}}$  values are higher than that of 2050-H.

Table 18 SF<sub>max</sub> and corresponding specific ESSN of different textures in Al alloys [41,42]

Br	ass	C	u		S	Go	oss	Cu	ıbe	R-C	ube
$SF_{max}$	ESSN	$SF_{max} \\$	ESSN								
0.408	2	0.272	6	0.422	1	0.408	8	0.408	8	0.408	4

Table 19 Calculated ESSN of different Al-Li alloy sheets and plates after solutionization

219	5-1	-1 2195-2		2A96		2A55		2050 sheet		
2 mm	5 mm	2 mm	5 mm	2 mm	10 mm	2 mm	10 mm	Н	L	A
4.30	3.56	4.69	3.11	4.93	4.07	5.03	3.62	4.68	5.01	5.17

**Table 20** Calculated ESSN of different layers in 2297-T87 and 2050-T83 Al–Li alloy thick plates

2297-T87						2050-T83	
T/16	T/8	<i>T</i> /4	3 <i>T</i> /8	T/2	T/6	T/3	T/2
4.65	5.36	4.72	3.24	3.95	5.23	5.13	4.52

## 4.3 Effect of grain shape

According to the  $\overline{M}_{3.5}$  and  $\overline{\rm ESSN}$  values as well as corresponding tensile properties, there still exist some exceptions. The YS of the aged and solutionized 2050-L and 2050-A is much higher and their elongation is obviously lower than those of the aged and solutionized 2050-H (Table 7 and Fig. 10), but their corrected  $\overline{M}_{3.5}$  values (Table 16) are only a little higher and  $\overline{\rm ESSN}$  values are also higher. In addition, the YS at T/16 layer of 2297-T87 Al–Li alloy plate is the lowest but its  $\overline{M}_{3.5}$  value is higher than that at T/8 layer. These exceptions indicate that some other factors should be further considered.

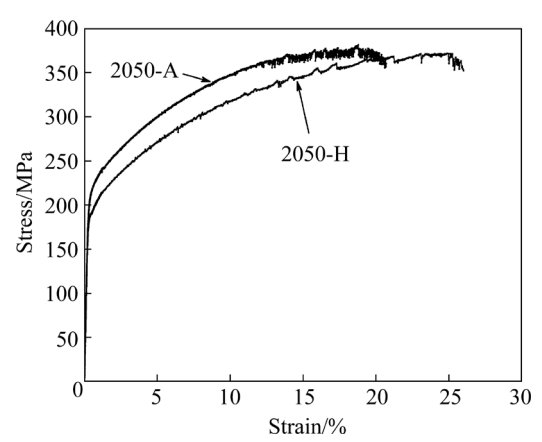


**Fig. 10** Tensile curves of solutionized 2050-A and 2050-H sheets

The 2050-H sheet is different from 2050-A and 2050-L sheets in the grain shape. The grain aspect ratio of 2050-H is much lower than that of 2050-L and 2050-A after solutionization, though all three sheets show full recrystallization features (Figs. 4(a, c)). It was reported that higher grain aspect ratio increased the alloy anisotropy [43,44]. The tensile deformation mechanism is dislocation slip accompanied with grain rotation. The elongated grains with jagged grain boundaries are difficult, but the equi-axed grains are easy to rotate [45]. Under macro-yielding stress, less slip systems are activated, but more grains rotate in the alloy with fine equi-axed grains. On the contrary, there are more activated slip systems and less grains rotating in the alloy with elongated grains and jagged grain boundaries.

Therefore, during the  $\overline{M}$  calculation, the Sachs model is more applicable for the alloy with equi-axed grains, but the Huctchinson model and Taylor model are more suitable for the alloys with elongated grains. As a result, the calculated  $\overline{M}_{3.5}$ 

value of 2050-H in Table 16 should be lower than 2.54, the calculated  $\overline{M}_{3.5}$  values are therefore rational to interpret the great YS difference among aged 2050-H, 2050-L and 2050-A sheets. Actually, because of different grain shapes in the outer layers and center layers of thick plate [21], the  $\overline{M}_{3.5}$  calculation also should use different models. In addition, in spite of their higher  $\overline{\rm ESSN}$  values, the non-rotation of large elongated grains lowers the elongation of the aged 2050-L and 2050-A sheets.

## **5 Conclusions**

- (1) For the 2195, 2A96, 2A55, 2050 and 2297 Al-Li alloys, higher  $\overline{M}$  values, which are mainly dependent on textures, in general correspond to higher YS. However, there still exist some exceptions in the alloy which contains high total volume fraction of recrystallization texture and texture-free component with high ratio of texture-free component fraction to recrystallization texture fraction.
- (2) During tensile deformation, some grains rotate and the activated slip system number is different in different grains. The  $\overline{M}$  calculation therefore should be corrected and normalized according to the assumption that dislocation slip is activated in only some grains, and single slip system is activated in the texture-free component with high fraction.
- (3) The grain shape plays an important role in YS and elongation, the higher aspect ratio tends to enhance the YS but lowers the elongation.
- $\underline{\text{(ESSN)}}$  ) affects the elongation, and higher  $\overline{\text{ESSN}}$  corresponds to larger elongation.

## References

- [1] RIOJA R J, LIU J. The evolution of Al–Li base products for aerospace and space applications [J]. Metallurgical and Materials Transactions A, 2012, 43: 3325–3337.
- [2] LI Jin-feng, NING hong, LIU Dan-yang, ZHENG Zi-qiao. Alloying and micro-alloying in Al-Cu-Li series alloys [J]. The Chinese Journal of Nonferrous Metals, 2021, 31(2): 258-279. (in Chinese)
- [3] GABLE B M, ZHU A W, CSONTOS A A, STARKE E A Jr. The role of plastic deformation on the competitive microstructural evolution and mechanical properties of a novel Al–Li–Cu–X alloy [J]. Journal of Light Metals, 2001, 1(1): 1–14.

- [4] GUMBMANN E, LEFEBVRE W, de GEUSER F, SIGLI C, DESCHAMPS A. The effect of minor solute additions on the precipitation path of an Al-Cu-Li alloy [J]. Acta Materialia, 2016, 115: 104-114.
- [5] MURAYAMA M, HONO K. Role of Ag and Mg on precipitation of T1 phase in an Al-Cu-Li-Mg-Ag alloy [J]. Scripta Materialia, 2001, 44: 701-706.
- [6] TSIVOULAS D, PRANGNELL P B. Comparison of the effect of individual and combined Zr and Mn additions on the fracture behavior of Al-Cu-Li alloy AA2198 rolled sheet [J]. Metallurgical and Materials Transactions A, 2014, 45: 1338-1351.
- [7] LEQUEU P, EBERL F, RHENALU A, JAMBU S, AVIATUBE A, WARNER T, DANIELOU A, BES B. Latest generation of Al–Li alloys developed by Alcan Aerospace [C]//Proceedings of the 1st European Conference on Materials and Structures in Aerospace (EUCOMAS). Berlin, Germany: VDI-VDE Verlag GmbH, 2008: 77–84.
- [8] GUINEL M J F, BRODUSCH N, SHA G, SHANDIZ M A, DEMERS H, TRUDEAU M, RINGER S P, GAUVIN R. Microscopy and microanalysis of complex nanosized strengthening precipitates in new generation commercial Al-Cu-Li alloys [J]. Journal of Microscopy, 2014, 255(3): 128-137.
- [9] WEI Xiu-yu, ZHENG Zi-qiao, SHE Ling-juan, CHEN Qiu-ni, LI Shi-chen. Microalloying roles of Mg and Zn additions in 2099 Al-Li alloy [J]. Rare Metal Materials and Engineering, 2010, 39(9): 1583–1587. (in Chinese)
- [10] LEE H S, NO K. Materials and manufacturing technology for aerospace application [J]. Key Engineering Materials, 2016, 707: 148–153.
- [11] ROMIOS M, TIRASCHI R, PARRISH C, BABEL H W, OGREN J R, ES-SAID O S. Design of multistep aging treatments of 2099 (C458) Al–Li alloy [J]. Journal of Materials Engineering and Performance, 2005, 14: 641–646.
- [12] BOIS-BROCHU A, BLAIS C, GOMA F A T, LAROUCHE D, BOSELLI J, BROCHU M. Effects of deformation texture intensities and precipitates on the anisotropy of mechanical properties of Al-Li alloy 2099-T83 extrusions [C]//Proceedings of the 13th International Conference on Aluminum Alloys (ICAA13). Pittsburgh, USA: TMS (The Minerals, Metals & Materials Society), 2012: 1831-1836.
- [13] BALDUCCI E, CESCHINI L, MESSIERI S, WENNER S, HOLMESTAD R. Effects of overaging on microstructure and tensile properties of the 2055 Al-Cu-Li-Ag alloy [J]. Materials Science and Engineering A, 2017, 707: 221-231.
- [14] LUO Xian-fu, ZHENG Zi-qiao, ZHONG Ji-fa, ZHANG Hai-feng, ZHONG Jing, LI Shi-chen, LI Jin-feng. Effects of Mg, Ag and Zn multialloying on aging behavior of new Al-Cu-Li alloy [J]. The Chinese Journal of Nonferrous Metals, 2013, 23(7): 1833–1842. (in Chinese)
- [15] LI Jin-feng, LIU Ping-li, CHEN Yong-lai, ZHANG Xu-hu, ZHENG Zi-qiao. Mechanical properties and microstructures of Mg, Ag and Zn mult-microalloyed Al-(3.2-3.8)Cu-(1.0-1.4)Li alloys [J]. Transactions of Nonferrous Metal Society of China, 2015, 25(7): 2103-2112.
- [16] LI Jin-feng, CHEN Yong-lai, ZHANG Xu-hu, LIU Qing, ZHENG Zi-qiao, YAO Yong, WANG Jian. Structures and mechanical properties of a super-high strength Al-Li alloy

- [J]. Rare Metal Materials and Engineering, 2017, 46(12): 3715–3720. (in Chinese)
- [17] MA Yun-long, LI Jin-feng, ZHANG Run-zhe, TANG Jian-guo, HUANG Cheng, LI Hong-ying, ZHENG Zi-qiao. Strength and structure variation of 2195 Al-Li alloy caused by different deformation processes of hot extrusion and cold-rolling [J]. Transactions of Nonferrous Metals Society of China, 2020, 30(4): 835–849.
- [18] VASUDEVAN A K, PRZYSTUPA M A, FRICKE W G. Texture-microstructure effects in yield strength anisotropy of 2090 sheet alloy [J]. Scripta Metallurgica et Materialia, 1990, 24: 1429–1434.
- [19] EL-ATY A A, XU Y, ZHANG S H, MA Y, CHEN D Y. Experimental investigation of tensile properties and anisotropy of 1420, 8090 and 2060 Al-Li alloys sheet undergoing different strain rates and fibre orientation: A comparative study [J]. Procedia Engineering, 2017, 207: 13–18.
- [20] VASUDEVAN A K, FRICKE W G, MALCOLM R C, BUCCI R J, BARLAT F. On through thickness crystallographic texture gradient in Al-Li-Cu-Zr alloy [J]. Metallurgical Transactions A, 1988, 19: 731-732.
- [21] WU P F, DENG Y L, ZHANG J, FAN S T, ZHANG X M. The effect of inhomogeneous microstructures on strength and fatigue properties of an Al-Cu-Li thick plate [J]. Materials Science and Engineering A, 2018, 731: 1–11.
- [22] XU X, HAO M, CHEN J, HE W, LI G, JIAO C, BURNETT T L, ZHOU X. Influence of microstructural and crystallographic inhomogeneity on tensile anisotropy in thick-section Al-Li-Cu-Mg plates [J]. Materials Science and Engineering A, 2022, 829: 142135.
- [23] LU Ding-ding, LI Jin-feng, NING Hong, MA Peng-cheng, CHEN Yong-lai, ZHANG Xu-hu, ZHANG Kai, LI Jian-mei, ZHANG Rui-feng. Effects of microstructure on tensile properties of AA2050-T84 Al-Li alloy [J]. Transactions of Nonferrous Metals Society of China, 2021, 31(5): 1189-1204.
- [24] WANG Hai-jin, ZHENG Zi-qiao, FAN Xue-song. Mechanical anisotropy and inhomogeneity through thickness of 2297-T87 Aluminum alloy thick plate [J]. Rare Metal Materials and Engineering, 2016, 45(5): 1196–1202. (in Chinese)
- [25] HAFLEY R A, DOMACK M S, HALES S J, SHENOY R N. Evaluation of aluminum alloy 2050-T84 microstructure and mechanical properties at ambient and cryogenic temperatures [R]. Hampton, Virginia: Langley Research Center, National Aeronautics and Space Administration, 2011.
- [26] TEMPUS G, CALLES W, SCHARF G. Influence of extrusion process parameters and texture on mechanical properties of Al–Li extrusions [J]. Materials Science and Technology, 1991, 7: 937–946.
- [27] MISHRA S, SURESH M, MORE A M, BISHT A, NAYAN N, SUWAS S. Texture control to reduce yield strength anisotropy in the third generation aluminum-copper-lithium alloy: Experiments and modeling [J]. Materials Science and Engineering A, 2021, 799: 140047.
- [28] CAI Wen-xin, LI Jin-feng, LU Ding-ding, LIU Dan-yang, NING Hong. Mechanical properties and structures variation of 2050 Al-Li alloy sheet caused by annealing prior to

- solution treatment [J]. Aerospace Materials and Technology, 2019, 49(6): 47–52. (in Chinese)
- [29] RAKSHIT R, SARKAR A, PANDA S K, MANDAL S. Influence of out-of-plane stretch forming induced different strain paths on micro-texture evolution, slip system activity and Taylor factor distribution in Al–Li alloy [J]. Materials Science and Engineering A, 2022, 830: 142267.
- [30] ZHANG Run-zhe, MA Yun-long, LIU Dan-yang, NING Hong, LI Jin-feng, CAI Chao. Dependence of mechanical properties and microstructures of 2195 Al–Li alloy on cold and hot deformation process [J]. Chinese Journal of Rare Metals, 2021, 45(2): 129–136. (in Chinese)
- [31] STARINK M J, WANG S C. A model for the yield strength of overaged Al–Zn–Mg–Cu alloys [J]. Acta Materialia, 2003, 51: 5131–5150.
- [32] MISHRA S, YADAVA M, KULKARNI K, GURAO N P. A modified Taylor model for predicting yield strength anisotropy in age hardenable aluminium alloys [J]. Materials Science and Engineering A, 2017, 699: 217–228.
- [33] STARINK M J, WANG P, SINCLAIR I, GREGSON P J. Microstructure and strengthening of Al-Li-Cu-Mg alloys and MMCs: II. Modelling of yield strength [J]. Acta Materialia, 1999, 47(4): 3855-3868.
- [34] XIANG Zheng-wu, LI Jin-feng, NING Hong, CHEN Yong-lai, ZHANG Xu-hu. Microstructure and strength contribution of T8-aged 2195 Al-Li alloy with different pre-stretching [J]. Aerospace Materials and Technology, 2021, 51(4): 140–146. (in Chinese)
- [35] ZENG G J, NING H, DENG S X, LI J F, YAO Y, GUO Y J, LU D D, LI Y Z, LIU Z H, MA P C, ZHANG R F. Quantification of the effect of increased pre-deformation on microstructure and mechanical properties of 2A55 Al–Li alloy [J]. Advanced Engineering Materials, 2022, 24(9): 2200033.
- [36] RODGERS B I, PRANGNELL P B. Quantification of the

- influence of increased pre-stretching on microstructure-strength relationships in the Al-Cu-Li alloy AA2195 [J]. Acta Materialia, 2016, 108: 55-67.
- [37] ZHANG N, TONG W. An experimental study on grain deformation and interactions in an Al-0.5%Mg multicrystal [J]. International Journal of Plasticity, 2004, 20: 523-542.
- [38] CHEN P, MAO S C, LIU Y, WANG F, ZHANG Y F, ZHANG Z, HAN X D. In-situ EBSD study of the active slip systems and lattice rotation behavior of surface grains in aluminum alloy during tensile deformation [J]. Materials Science and Engineering A, 2013, 580: 114–124.
- [39] BRIDIER F, VILLECHAISE P, MENDEZ J. Analysis of the different slip systems activated by tension in a  $\alpha/\beta$  titanium alloy in relation with local crystallographic orientation [J]. Acta Materialia, 2005, 53: 555–567.
- [40] ZHAO Q, LIU Z Y, WAHAB M A. Enhanced Brass texture of hot-rolled Al-4Cu-1.6Mg alloy by 0.1% Zr addition [J]. Materials Characterization, 2020, 169: 110643.
- [41] XU Yong-qian, ZHAN Li-hua, HUANG Ming-hui, LIU Chun-hui, WANG Xun. Anisotropy in creep-ageing behavior of textured Al-Cu-Mg alloy [J]. International Journal of Lightweight Materials and Manufacture, 2018, 1: 40-46.
- [42] BIAN T J, LI H, YANG J C, LEI C, WU C H, ZHANG L W, CHEN G Y. Through-thickness heterogeneity and in-plane anisotropy in creep aging of 7050 Al alloy [J]. Materials and Design, 2020, 196: 109190.
- [43] CHO K K, KWUN S I, CHUNG Y H, LEE C W, SHIN M C. Effects of grain shape and texture on the yield strength anisotropy of Al–Li alloy sheet [J]. Scripta Materialia, 1999, 40(6): 651–657.
- [44] CHUNG Y H, CHO K K, HAN J H, SHIN M C. Effect of grain shape and texture on the earings in Al–Li alloy [J]. Scripta Materialia, 2000, 43: 759–764.
- [45] LI chong. Study on low-cycle fatigue for zirconium alloys [D]. Chengdu: Sichuan University, 2003: 62–64.

## 铝锂合金晶粒组织与拉伸性能的关系

李昊然1, 邹智涛1, 李劲风1,2, 徐国富1,2, 郑子樵1

- 1. 中南大学 材料科学与工程学院,长沙 410083;
- 2. 中南大学 有色金属材料科学与工程教育部重点实验室, 长沙 410083

摘 要:从新的视角对部分铝锂合金晶粒组织(织构和晶粒形状)与屈服强度和伸长率的相关性进行研究。研究材料包括 2195、2A96、2A55 及 2050 铝锂合金 2 mm 厚度薄板和 5 mm 与 10 mm 厚度板材以及厚度为 80~85 mm 具有不同厚度层的 2297-T87 和 2050-T83 铝锂合金厚板。较高取向因子平均值( $\overline{M}$ )一般对应较高的屈服强度,但存在一些例外。由于拉伸屈服时不同晶粒内启动滑移系数量不同,而且部分晶粒只发生转动,因此, $\overline{M}$  值计算时应在剔除无滑移系激活的晶粒并考虑最易激活滑移系的基础上进行修正及归一化处理。同时,晶粒形状对铝锂合金屈服强度有重要影响;尽管几乎发生完全再结晶,但晶粒长厚比增加时,晶粒转动困难,塑性屈服需启动更多滑移系,从而有利于提高铝锂合金屈服强度。另外,上述铝锂合金的伸长率与总等效滑移系数量及晶粒形状直接相关,增加总等效滑移系数量或降低晶粒长厚比低均有利于伸长率的提高。

关键词: 铝锂合金; 屈服强度; 伸长率; 织构; 晶粒形状; 滑移系